Simultaneous Estimation of Shape and Motion of an Asteroid for Automatic Navigation

Naoya Takeishi[1], Takehisa Yairi[1],
Yuichi Tsuda[2], Fuyuto Terui[2], Naoko Ogawa[2] and Yuya Mimasu[2]

***Abstract*— In an asteroid exploration and sample return mission, accurate estimation of the shape and motion of the target asteroid is essential for selecting a touchdown site and navigating a spacecraft during touchdown operation. In this work, we present an automatic estimation method for the shape and motion of an asteroid, which is planned to be tested in future exploration missions including Japanese Hayabusa-2 [1]. Our task is to estimate the shape and rotation axis of the asteroid, as well as positions of the spacecraft from optical images. The proposed method is based on the expectation conditional-maximization (ECM) framework that consists of an auxiliary particle filter and nonlinear optimization techniques. One of our technical contributions is the estimation of the direction of rotation axis of the asteroid from monocular camera images, which are taken by the moving spacecraft. We conducted two experiments with synthetic data and an asteroid mock-up to show the validity of the proposed method and to present the numerical accuracy.**

I. INTRODUCTION

Asteroid touchdown and sample return are one of the most exciting and challenging space exploration missions. In the past related missions such as Japanese asteroid exploration by Hayabusa, large parts of the spacecraft navigation in the approaching phase were conducted manually by the operators on the ground [2]. Needless to say, a fully autonomous navigation is desirable in the upcoming missions, from the viewpoints of operator's workload. Indispensable elements in the vision-based autonomous navigation are the geometric model and the detail of rotation axis of the target asteroid. As it is impossible to estimate them precisely by direct observation from the earth, we have to do it from the optical images sent by the spacecraft after it arrives in the proximity of the asteroid. However, this estimation is not straightforward since not only the asteroid's shape and motion, but also the spacecraft's pose are uncertain.

We are developing a fully automatic image-based navigation for future asteroid exploration missions, and planning to test the new method in the mission of Japanese asteroid explorer Hayabusa-2 [1]. So far, we presented a performance evaluation of landmark tracking techniques for asteroids [3], and an experimental work on fast geometry estimation using an improved matrix factorization [4]. In this work, we proposed a core part of an automatic navigation, that is, the estimation of asteroid's shape and direction of rotation axis using only an optical camera. Generally, a similar estimation problem has been intensively studied and referred to as monocular simultaneous localization and mapping (monocular SLAM) [5]. One of our technical contributions is the modification for rotation axis estimation in a monocular SLAM framework. We briefly introduced related literatures in Section II.

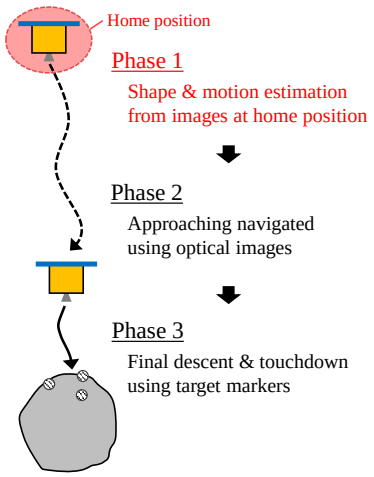

Fig. 1. A brief summary of a scenario of a touchdown on an asteroid. In this work, we focus on shape and motion estimation in Phase 1. Note that the definition of Phases 1-3 is not general, and used only in this paper for clarity.

A summary of a touchdown on an asteroid is depicted in Figure 1. We defined Phases 1-3 for a descriptive purpose in this paper, though we believe that this definition fits actual missions in the past and the future. We assumed that a spacecraft stays in a certain narrow area called "home position" above the rotating asteroid to take its images and to estimate the shape and motion (Phase 1). Then, the spacecraft descends to a touchdown site navigated using the asteroid images (Phase 2). Approaching close enough to the asteroid surface, the spacecraft is navigated using target markers until touchdown (Phase 3). In this work, we focused on Phase 1 where active range sensors such as LIDAR do not work due to a large distance between the spacecraft and the asteroid, and that is why we developed a monocular framework. The estimation will be processed on the ground, due to a restricted computational resource of the spacecraft. Hence, the estimation is done offline (a batch solution). The problem is formulated at length in Section III.

The proposed method is based on the expectation

[1] Naoya Takeishi and Takehisa Yairi are with Department of Aeronautics and Astronautics, the University of Tokyo, Tokyo, Japan. {takeishi, yairi}@space.rcast.u-tokyo.ac.jp

[2] Yuichi Tsuda, Fuyuto Terui, Naoko Ogawa and Yuya Mimasu are with Japan Aerospace Exploration Agency, Sagamihara, Japan.

conditional-maximization (ECM) framework [6], in which unknowns are iteratively updated until convergence. We utilized an auxiliary particle filter to infer positions of a spacecraft, while learning asteroid's shape and direction of rotation axis by nonlinear optimization techniques. Details of the proposed method are described in Section IV, and experimental results are presented in Section V.

II. RELATED WORK

The simultaneous localization and mapping (SLAM) has been intensively studied in the robotics community for decades [5]. In a general SLAM framework, a process model and an observation model are given. The process model presents a transition probability of robot's states, and the observation model tells how features are observed by the robot. The SLAM problem is commonly solved using filtering and smoothing techniques. For instance, FastSLAM 2.0 [7] utilizes a Rao-Blackwellized particle filter with an improved proposal distribution, and incremental smoothing and mapping (iSAM) [8] provides a smoothed solution with linearized least squares.

There is a similar problem termed structure from motion (SFM) in the area of computer vision [9]. The SFM refers to a simultaneous estimation of camera poses and geometry of a scene, and differs from the SLAM in that the SFM does not require a model of camera's kinematics or dynamics. The SFM techniques often utilize nonlinear optimization, in which projection errors of landmarks are minimized.

Several researchers have proposed methods for localization or for mapping with a rotating object. Bayard and Brugarolas [10] presented an on-board monocular localization method for small body explorations. Augenstein and Rock [11] proposed a robust localization and mapping technique for a tumbling target. Cocaud and Kubota [12] have shown an image-based navigation technique for small celestial bodies based on RBPF-SLAM. However, these techniques do not explicitly estimate motion parameters of a target. There are some papers and thesis [13], [14], [15] that succeed at estimating motion parameters, while they use range sensors like a laser camera and a stereo camera, instead of bearing (monocular) sensors.

III. PROBLEM FORMULATION

This section gives a problem formulation for shape and motion estimation of an asteroid. We dealt with a SLAM problem with a spacecraft hovering above the rotating asteroid. The spacecraft is slightly moving and controlled to bring the asteroid into the center of the field of vision as depicted in Figure 2. Thus, a dominant transition factor is the asteroid's rotation, and we treated the slight movement of the spacecraft as a noise.

We assumed that the asteroid is rotating around a fixed single axis without nutation, since there are some suggestions of single axis spin of the asteroid 1999JU3, the target of Hayabusa-2, such as [16]. Asteroid's angular velocity is supposed to be known in this paper, because the rotational period can be estimated on the ground using lightcurve

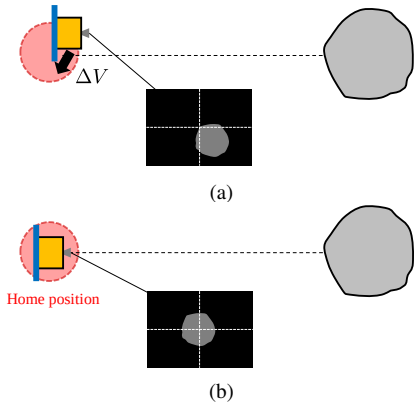

Fig. 2. A schema of spacecraft's control policy above the asteroid (Phase 1). The spacecraft manages to bring the asteroid into the center of its field of vision like (a) $\rightarrow$ (b). The scales in this figure are not correct.

data. For example, the rotational period of asteroid 1999JU3 is estimated to be approximately 7.63[hours] [17], [18]. Moreover, we assumed that the center of mass and the geometric center are at almost the same point in the asteroid. Hence, the motion parameter to be estimated is the direction of rotation axis, which is difficult to estimate accurately by direct observations from the earth.

We formulated the problem as shown in Figure 3. The Markovian state $\mathbf{x}_k$ $(k = 1,\ldots,M)$ is the kth spacecraft pose, which consists of a unit quaternion q_k and a translation vector $\mathbf{t}_k$. The kth state represents a coordinate transformation from the asteroid-fixed frame to the kth camera-fixed frame. Note that the subscript k denotes a time and M is the number of states, that is, the number of images to be used. The rotation axis of the asteroid is represented in a vector $\mathbf{r}$ $(||\mathbf{r}||_2 = 1)$, and it affects the transition of the states $\mathbf{x}$. The parameter $\mathbf{z}^{(n)}$ $(n = 1,\ldots,N)$ denotes the 3-D location of the nth landmark on the asteroid surface, and the observation $\mathbf{y}_k^{(n)}$ denotes the 2-D location of the nth landmark observed by the spacecraft with the kth pose (that is, a set $\{\mathbf{y}_k\}$ corresponds to the kth image). The input u_k is the time interval between the $(k-1)$th and the kth images. Our task is to infer $\mathbf{x}$ and to learn $\mathbf{r}$ and $\mathbf{z}$ from the observations $\mathbf{y}$.

A. Transition model

The transition model used in this work is a kinematic property of the spacecraft and the asteroid. This formulation is useful because it can be calculated exactly in discrete time. However, it requires an assumption that the rotation axis observed by the spacecraft is almost constant, and it holds when the total photographing period is short enough compared to asteroid's revolution period.

The transition model $\mathbf{x}_k = f(\mathbf{x}_{k-1}, \mathbf{r})$ is given by the asteroid's rotation and the noises as shown in Figure 4, and formulated as follows:

$$q_k = \bar{q}_{v_r} \bar{q}_{u_k} q_{k-1}, \quad (1)$$

$$\mathbf{t}_k = \mathbf{t}_{k-1} + \mathbf{v}_t, \quad (2)$$

where q_{u_k} represents asteroid's rotation within the time interval u_k around the axis $\mathbf{r}$, and q_{v_r} and $\mathbf{v}_t$ are noises of

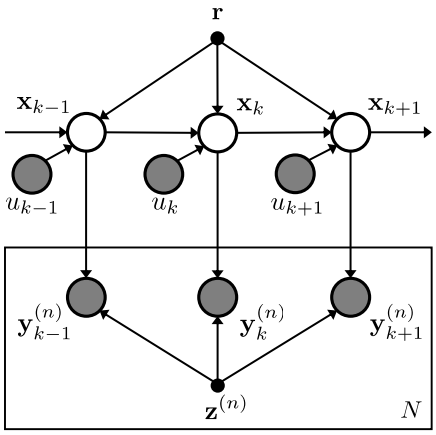

Fig. 3. The problem formulation graphically represented. $\mathbf{x}_k$ is the kth state of the spacecraft. $\mathbf{r}$ is the axis of rotation. $\mathbf{z}^{(n)}$ is the 3-D location of the nth landmark. $\mathbf{y}_k^n$ is the 2-D location of the observed nth landmark. u_k represents a time interval between kth and $(k-1)$th states.

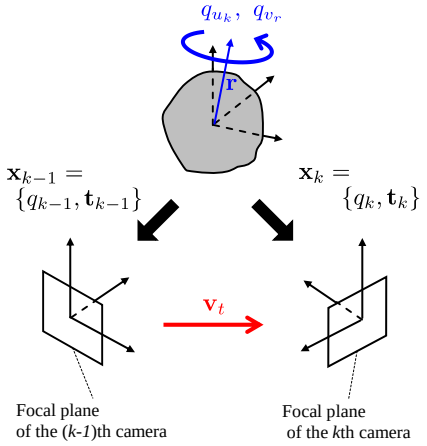

Fig. 4. A diagram of the transition model. Within the observation interval $(k-1) \to k$, the asteroid-fixed frame rotates by q_{u_k} with a noise q_{v_r}, whereas the camera-fixed frame slightly moves by a noise $\mathbf{v}_t$. The states $\mathbf{x}$ that undergo the transition denote coordinate transformations from the asteroid-fixed frame to the camera-fixed frames.

the rotation and translation, respectively. Note that q_{v_r}, q_{u_k} and q_k $(k = 1, ..., M)$ are unit quaternions, and $\bar{q}$ denotes an inverse quaternion of q.

The rotational noise q_{v_r} is given by a Gaussian random variable $\mathbf{v}_r \sim \mathcal{N}(\mathbf{0}, \Sigma_r), \mathbf{v}_r \in \mathbb{R}^3$ as in the literature [19]:

$$\begin{aligned} q_{v_r} &= [q_0 \ \mathbf{q}], \\ q_0 &= ||\mathbf{v}_r||, \\ \mathbf{q} &= [q_1 \ q_2 \ q_3]^T = \mathbf{v}_r / ||\mathbf{v}_r||, \end{aligned}$$

and the translational noise follows a Gaussian $\mathbf{v}_t \sim \mathcal{N}(0, \Sigma_t)$. The translational noise represents the slight moving of the spacecraft whereas the rotational noise is for uncertainty of the axis of rotation.

Note that the transition model can be extended to consider dynamics of the spacecraft, which enables us to deal with more complicated scenarios including a controlled observation tour to estimate the shape of a nutating asteroid.

B. Observation model

The observation model $\mathbf{y}_k^{(n)} = h(\mathbf{x}_k, \mathbf{z}^{(n)})$ is given by a pin-hole camera model with a Gaussian observation noise $\mathbf{v}_o \sim \mathcal{N}(0, \Sigma_o)$:

$$\tilde{\mathbf{y}}_k^{(n)} = K[R(q_k)|\mathbf{t}_k]\tilde{\mathbf{z}}^{(n)} + [\mathbf{v}_o^T \ 1]^T, \tag{3}$$

where K is camera's intrinsic matrix, and the extrinsic matrix $[R(q_k)|\mathbf{t}_k]$ is

$$\begin{pmatrix} q_0^2+q_1^2-q_2^2-q_3^2 & 2(q_1q_2+q_0q_3) & 2(q_1q_3-q_0q_2) & t_1 \\ 2(q_1q_2-q_0q_3) & q_0^2-q_1^2+q_2^2-q_3^2 & 2(q_2q_3+q_0q_1) & t_2 \\ 2(q_1q_3+q_0q_2) & 2(q_2q_3-q_0q_1) & q_0^2-q_1^2-q_2^2+q_3^2 & t_3 \\ 0 & 0 & 0 & 1 \end{pmatrix}.$$

Note that $\tilde{\mathbf{y}}_k^{(n)}$ and $\tilde{\mathbf{z}}^{(n)}$ are in homogeneous coordinates.

IV. PROPOSED METHOD

The proposed estimation method consists of an auxiliary particle filter to infer $\mathbf{x}$, a minimization of projection error to learn $\mathbf{z}$, and a minimization of transition error to learn $\mathbf{r}$. These inferring and learning techniques are iteratively run in turn until a convergence. In the following subsections, we explain each part of the proposed method and the overall procedure.

Tracking landmarks is out of the scope of this paper, while one can detect and track landmarks using keypoint detectors and local descriptors such as SIFT [23], and eliminate outliers using RANSAC [24].

A. Auxiliary particle filtering

We adopted a filtering distribution $p(\mathbf{x}_k|\mathbf{y}_{1:k}, \mathbf{z}, \mathbf{r})$ for an estimator of $\mathbf{x}_k$, with fixed $\mathbf{z}$ and $\mathbf{r}$. An auxiliary particle filter (APF) is used to provide the filtering distribution, where the transition model is given by Equations (1) and (2) and the observation model is given by Equation (3). We used a standard procedure of the APF on which one can find a detailed description in the literatures such as [20].

B. Observation error minimization

To get a maximum likelihood estimation of $\mathbf{z}^{(n)}$, we minimized the squared observation error using the model given in Equation 3:

$$\mathbf{z}^{(n)} = \arg\min_{\mathbf{z}^{(n)}} \sum_k ||\mathbf{y}_k^{(n)} - h(E_k[\mathbf{x}_k], \mathbf{z}^{(n)})||_2^2, \tag{4}$$

where $E_k[\cdot]$ denotes an expected value under the filtering distribution $p(\mathbf{x}_k|\mathbf{y}_{1:k}, \mathbf{z}, \mathbf{r})$. This optimization can be done with a general solver, while we used the Levenberg-Marquardt (LM) algorithm [21]. When the nth landmark $\mathbf{z}^{(n)}$ is observed first time, the LM algorithm is initialized with a direct linear transform (DLT) algorithm [22].

C. Transition error minimization

The preceding two steps are commonly used in other methods concerning localization and mapping. Additionally, we did another optimization to estimate the rotation axis $\mathbf{r}$

1: **procedure** ESTIMATION
2: **for** $k = 2, \ldots, M$ **do** ▷ Initialization (Multicycle ECM)
3: **repeat**
4: $p(\mathbf{x}_k|\mathbf{y}_{1:k}) \leftarrow \text{APFSTEP}(p(\mathbf{x}_{k-1}|\mathbf{y}_{1:k-1}), \mathbf{y}_k)$
5: $\mathbf{z}^{(n)} \leftarrow$ Equation 4
6: $\mathbf{r} \leftarrow$ Equation 5
7: **until** convergence
8: **end for**
9: **repeat** ▷ Main iteration (ECM)
10: **for** $k = 2, \ldots, M$ **do**
11: $p(\mathbf{x}_k|\mathbf{y}_{1:k}) \leftarrow \text{APFSTEP}(p(\mathbf{x}_{k-1}|\mathbf{y}_{1:k-1}), \mathbf{y}_k)$
12: **end for**
13: $\mathbf{z}^{(n)} \leftarrow$ Equation 4
14: $\mathbf{r} \leftarrow$ Equation 5
15: **until** convergence
16: **end procedure**

Fig. 5. The overall estimation procedure. Please note that $\mathbf{r}$ and $\mathbf{z}$ were dropped in a filtering distribution $p(\mathbf{x}_k|\mathbf{y}_{1:k}, \mathbf{z}, \mathbf{r})$ for simplicity. APFSTEP$(\cdot)$ is a step of the auxiliary particle filter that updates the estimation of $\mathbf{x}$.

robustly albeit the small moving, using the transition factor f given at Equations 1 and 2:

$$\mathbf{r} = \arg\min_{\mathbf{r}} \sum_{l=2}^{k} ||E_l[\mathbf{x}_l] - f(E_{l-1}[\mathbf{x}_{l-1}])||_2^2, \tag{5}$$

which can be solved with the same method as that used in the projection error minimization. This *transition error minimization* are reasonable in the sense that the rotation axis $\mathbf{r}$ is independent of $\mathbf{y}$ and $\mathbf{z}$ given the states $\mathbf{x}$ as shown in Figure 3, and it can estimate the rotation axis robustly canceling spacecraft's small moving by smoothing transition errors.

There are some alternatives such as dual filtering, joint filtering and smoothing to estimate the axis of rotation, and we have tried these methods. However, we empirically found that in our problem setting, filtering and smoothing did not converge or failed to give a correct solution, probably due to the small moving of the camera.

D. The overall method

The overall method is described in Figure 5. To estimate all unknown variables and parameters, we iteratively ran the three inferring and learning procedures: the APF for $\mathbf{x}$, the projection error minimization for $\mathbf{z}$, and the transition error minimization for $\mathbf{r}$.

The initial state $\mathbf{x}_1$ is given arbitrarily to define the asteroid-fixed frame, and the initial guess for $\mathbf{r}$ can be roughly given by an operator or with observation from the earth, but we do not have an initial solution of $\mathbf{z}$. Therefore, at the first stage of the method, the inferring and learning are iterated with every pair of images (Line 2–8). After that, the main iteration is run for all images (Line 9–15), in which every filtering distribution of $\mathbf{x}_k$ is inferred (Line 10–12) followed by minimizations with regard to $\mathbf{z}$ and $\mathbf{r}$ (Line 13,14). Note that the initialization is a kind of the multicycle ECM algorithms and the main iteration corresponds to the ECM algorithm [6].

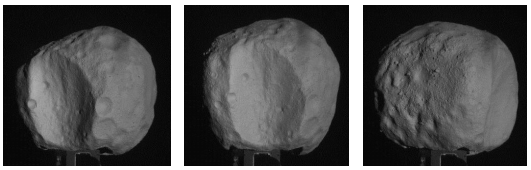

Fig. 6. Examples of images of an asteroid mock-up.

V. EXPERIMENTAL RESULTS

We conducted experiments using synthetic data and images of an asteroid mock-up. The experiment with synthetic data is to confirm the validity of the proposed method and to evaluate the accuracy numerically. Moreover, we made an asteroid mock-up as shown in Figure 6 and took its images to evaluate the proposed method in more realistic situation. In the following subsections, settings of data, parameters of experiments, and their results are described.

A. Synthetic data

We generated a dataset where 100 landmarks are scattered on the surface of a unit sphere centered at $[0\ 0\ 0]^T$. The sphere rotates at a constant angular velocity 5[deg/s], by the axis of rotation $\mathbf{r} = [-0.099\ 0.99\ 0.099]^T$. The state $\mathbf{x}$ evolves according to the process model (Equations 1 and 2), with noise covariances $\Sigma_r = 0, \Sigma_t = \text{diag}(10^{-4}, 10^{-4}, 10^{-4})$[px^2]. The initial position $\mathbf{x}_1$ was $q_1 = [1\ 0\ 0\ 0]$ and $\mathbf{t}_1 = [0\ 0\ 20]^T$[px]. This setting corresponds to a spacecraft observing an asteroid with a diameter of 1[km], at a remove of 20[km].

The landmarks are observed every 1 second (i.e. $u = 1$[sec]) while observations are missed when the landmarks are on far side of the sphere, or missed randomly even on nearside of the sphere, and the random missing probability was set $p = 0.25$ in this experiment. The observation follows the model given by Equation 3 where Σ_o was set to be $\text{diag}(1,1)$[px^2], and there assumed no errors in the data association. Camera's angle of view was set to 6[deg].

We applied the proposed method with the initial guess of rotation axis $\mathbf{r}_{init} = [0\ 1\ 0]^T$ and the number of particles $N_p = 2000$. An instance of the results are shown in Figures 7 and 8. Figure 7(a) is an instance of the estimated shape, and there is some parallel shifts between the estimated position of landmarks and the ground truth. Figure 7(b) is the same instance of the estimated shape that is registered to the ground truth using the iterative closest point algorithm. After 20 trials, the mean of RMS errors between the registered estimations and the ground truth was 9.7×10^{-3}[px] and the standard deviation was 2.6×10^{-3}[px]. We can tell that the relative position of landmarks were successfully estimated while a parallel shift remained.

Figure 8 shows the error angle between the estimations and the ground truth of the rotation axis along iterations. We can see that the estimation successfully converges to the ground truth.

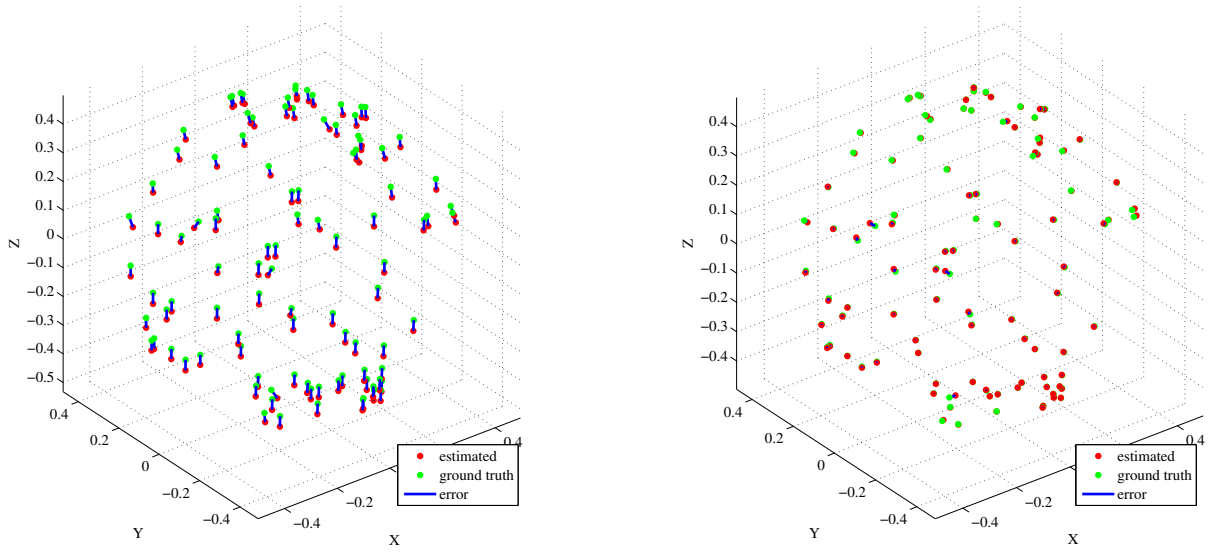

(a) (b)

Fig. 7. An instance of experimental results with synthetic data. (a) shows the estimated positions of landmarks (red points) that shift parallel from the ground truth (green points). (b) shows the estimated positions that were registered to the ground truth using the iterative closest point algorithm. We can tell that the relative position of landmarks were successfully estimated while a parallel shift remained. The unit of the axes is [px].

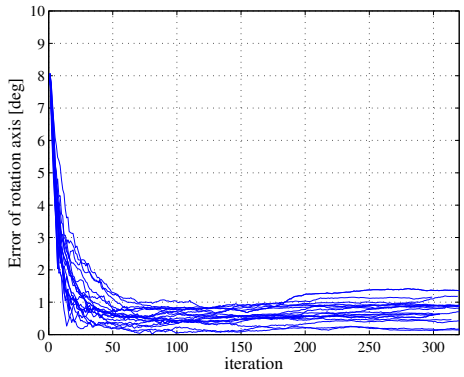

Fig. 8. Convergence of rotation axis on 20 trials. The vertical axis represents the error angle between the estimated and the true axis of rotation, and the horizontal axis represents the number of iterations.

B. Asteroid mock-up

We conducted another experiment with 72 images of the asteroid mock-up (Figure 6). These 1024×1024[px] images were taken using a fixed camera, with the mock-up rotated by 5[deg] each image. The imaging situation corresponds to the Hayabusa-2 spacecraft observing the target asteroid 1999JU3 at a distance of 23.59 [km]. In addition to the natural noises of the mock-up images, artificial disturbances that follows a Gaussian $\mathcal{N}(\mu = \mathbf{0}, \sqrt{\Sigma} = \mathrm{diag}(4,4))$[px] were given to each image to emphasize observer's slight moving. The vertical side of the mock-up is about 40[cm].

Before applying the proposed method, landmarks were configured on the surface of the mock-up using the scale-invariant feature transform (SIFT) [23]. We extracted SIFT keypoints, matched them with outlier elimination by the RANSAC [24], and built a graph where each vertex corresponds to a keypoint and each edge corresponds to a match. This graph consists of many connected components, and each component corresponds to a set of keypoints that are located at a certain distinct site (landmark) on the surface. We sorted the connected components by the number of edges, and selected the top 400 components as landmarks to use. Examples of the configured landmarks are shown in Figure 9.

Applying the proposed method, we show an instance of the estimated shape in Figure 10. We investigated the error between the estimated shapes and the ground truth measured by a laser scanner using the iterative closest point algorithm. After 10 trials, the mean of RMS errors was 18.4[mm] and the standard deviation was 2.2[mm].

VI. CONCLUSION

In this work, we presented a method for estimation of asteroid's shape and motion, which is planned to be tested in the future exploration. The proposed method is based on the auxiliary particle filtering and nonlinear optimization techniques, and updates spacecraft's state, asteroid's shape and the rotation axis iteratively. We showed experimental results with the synthesized dataset and the asteroid mock-up. In both cases, the validity of the proposed method was confirmed.

The method presented in this work is a core part of an automatic shape and motion estimation and descent navigation for asteroid explorations. Further research has to be done to improve the accuracy, robustness and computational speed.

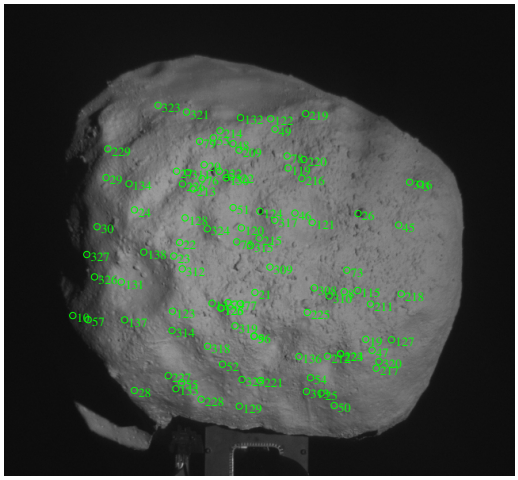

Fig. 9. Examples of the configured landmarks on an asteroid mock.

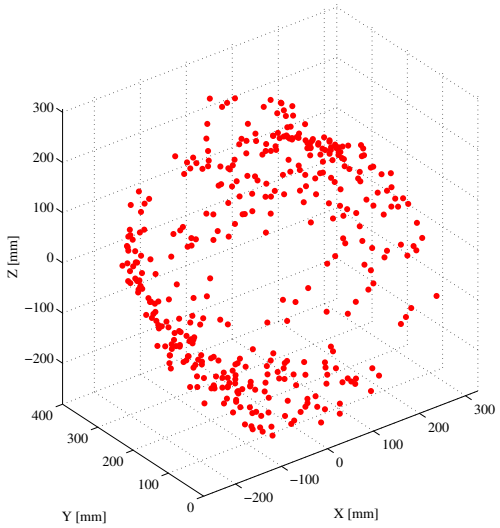

Fig. 10. An instance of the estimated shape of an asteroid mock-up. Note that the top of the mock-up directs to $Y+$.

REFERENCES

[1] Y. Tsuda, M. Yoshikawa, M. Abe, H. Minamino, and S. Nakazawa, "System design of the Hayabusa 2 – asteroid sample return mission to 1999 JU3," *Acta Astronautica*, vol. 90, pp. 356–362, 2013.

[2] K. Shirakawa, H. Morita, M. Uo, T. Hashimoto, T. Kubota, and J. Kawaguchi, "Accurate landmark tracking for navigating Hayabusa prior to final descent," in *Advances in the Astronautical Sciences*, vol. 124, 2006, pp. 1817–1826.

[3] N. Takeishi, A. Tanimoto, T. Yairi, Y. Tsuda, F. Terui, N. Ogawa, and Y. Mimasu, "Evaluation of interest-region detectors and descriptors for automatic landmark tracking on asteroids," *Transactions of the Japan Society for Aeronautical and Space Sciences*, vol. 58, no. 1, pp. 45–53, 2015.

[4] A. Tanimoto, N. Takeishi, T. Yairi, Y. Tsuda, F. Terui, N. Ogawa, and Y. Mimasu, "Fast estimation of asteroid shape and motion for spacecraft navigation," in *2013 IEEE International Conference on Robotics and Biomimetics (ROBIO)*, 2013, pp. 1550–1555.

[5] S. Thrun, W. Burgard, and D. Fox, *Probabilistic Robotics*. The MIT Press, 2005.

[6] X.-L. Meng and D. B. Rubin, "Maximum likelihood estimation via the ECM algorithm: A general framework," *Biometrika*, vol. 80, pp. 267–278, 1993.

[7] M. Montemerlo, S. Thrun, D. Koller, and B. Wegbrei, "FastSLAM 2.0: An improved particle filtering algorithm for simultaneous localization and mapping that provably converges," in *Proceedings of the Sixteenth International Joint Conference on Artificial Intelligence (IJCAI)*, 2003, pp. 1151–1156.

[8] M. Kaess, A. Ranganathan, and F. Dellaert, "iSAM: Incremental smoothing and mapping," *IEEE Transactions on Robotics*, vol. 24, pp. 1365–1378, 2008.

[9] R. Szeliski, *Computer Vision: Algorithms and Applications*. Springer, 2010.

[10] D. S. Bayard and P. B. Brugarolas, "On-board vision-based spacecraft estimation algorithm for small body exploration," *IEEE Transactions on Aerospace and Electronic Systems*, vol. 44, pp. 243–260, 2008.

[11] S. Augenstein and S. M. Rock, "Improved frame-to-frame pose tracking during vision-only sSLAM/SFM with a tumbling target," in *Proceedings of 2011 IEEE International Conference on Robotics and Automation (ICRA)*, 2011, pp. 3131–3138.

[12] C. Cocaud and T. Kubota, "Monocular SLAM-based navigation for autonomous approach descent and landing on small celestial bodies," in *International Symposium on Artificial Intelligence, Robotics and Automation in Space*, 2012.

[13] M. D. Lichter and S. Dubowsky, "State, shape and parameter estimation of space objects from range images," in *Proceedings of 2004 IEEE International Conference on Robotics and Automation (ICRA)*, 2004, pp. 2974–2979.

[14] F. Aghili, "A prediction and motion-planning scheme for visually guided robotic capturing of free-floating tumbling objects with uncertain dynamics," *IEEE Transactions on Robotics*, vol. 28, pp. 634–649, 2012.

[15] B. E. Tweddle, "Computer vision-based localization and mapping of an unknown, uncooperative and spinning target for spacecraft proximity operations," Ph.D. dissertation, The Massachusetts Institute of Technology, 2013.

[16] T. G. Müller, J. Ďurech, S. Hasegawa, M. Abe, K. Kawakami, T. Kasuga, D. Kinoshita, D. Kuroda, S. Urakawa, Y. S. S. Okumura7, S. Miyasaka, Y. Takagi, P. R. Weissma, Y.-J. Choi, S. Larson, K. Yanagisawa, and S. Nagayama, "Thermo-physical properties of 162173 (1999 JU3), a potential flyby and rendezvous target for interplanetary missions," *Astronomy & Astrophysics*, vol. 525, no. A145, 2011.

[17] M. Abe, K. Kawakami, S. Hasegawa, D. Kuroda, M. Yoshikawa, T. Kasuga, K. Kitazato, Y. Sarugaku, D. Kinoshita, S. Miyasaka, S. Urakawa, S. Okumura, Y. Takagi, N. Takato, T. Fujiyoshi, H. Terada, T. Wada, Y. Ita, F. Vilas, P. Weissman, Y.-J. Choi, S. Larson, S. Bus, and T. Mueller, "Ground-based observational campaign for asteroid 162173 1999 JU3," in *37th COSPAR Scientific Assembly*, ser. COSPAR Meeting, vol. 37, 2008, p. 12.

[18] M.-J. Kim, Y.-J. Choi, H.-K. Moon, M. Ishiguro, S. Mottola, M. Kaplan, D. Kuroda, D. S. Warjurkar, J. Takahashi, and j. . Yong-Ik Byun title = Optical observations of NEA 162173 (1999 JU3) during the 2011-2012 apparition.

[19] E. Kraft, "A quaternion-based unscented Kalman filter for orientation tracking," in *Proceedings of the Sixth International Conference of Information Fusion*, 2003, pp. 47–54.

[20] M. K. Pitt and N. Shephard, "Filtering via simulation: Auxiliary particle filters," *Journal of the American Statistical Association*, vol. 94, pp. 590–599.

[21] D. W. Marquardt, "An algorithm for least-squares estimation of nonlinear parameters," *Journal of the Society for Industrial and Applied Mathematics*, vol. 11, pp. 431–441, 1963.

[22] R. I. Hartley and A. Zisserman, *Multiple View Geometry in Computer Vision*, 2nd ed. Cambridge University Press, 2004.

[23] D. G. Lowe, "Distinctive image features from scale-invariant keypoints," *International Journal of Computer Vision*, vol. 60, pp. 91–110, 2004.

[24] M. A. Fischler and R. C. Bolles, "Random sample consensus: A paradigm for model fitting with applications to image analysis and automated cartography," *Communications of the ACM*, vol. 24, pp. 381–395, 1981.